Available online at www.sciencedirect.com
SCIENCE DIRECT®
Advances in Water Resources 27 (2004) 1135–1150
Advances in Water Resources
www.elsevier.com/locate/advwatres

Carbon and water cycling in a Bornean tropical rainforest under current and future climate scenarios

Tomo'omi Kumagai [a,b,*], Gabriel G. Katul [b,c], Amilcare Porporato [c], Taku M. Saitoh [d], Mizue Ohashi [e], Tomoaki Ichie [f], Masakazu Suzuki [g]

[a] University Forest in Miyazaki, Kyushu University, Shiiba-son, Miyazaki 883-0402, Japan
[b] Nicholas School of the Environment and Earth Sciences, Box 90328, Duke University, Durham, NC 27708-0328, USA
[c] Department of Civil and Environmental Engineering, Box 90287, Duke University, Durham, NC 27708-0287, USA
[d] Research Institute of Kyushu University Forest, Sasaguri, Fukuoka 811-2415, Japan
[e] Faculty of Forestry, University of Joensuu, Joensuu 80101, Finland
[f] Center for Tropical Forest Science—Arnold Arboretum, Asia Program, NIE-NTU 637616, Singapore
[g] Graduate School of Agricultural and Life Sciences, The University of Tokyo, Tokyo 113-8657, Japan

Received 29 April 2004; received in revised form 5 October 2004; accepted 8 October 2004

Abstract

We examined how the projected increase in atmospheric CO_2 and concomitant shifts in air temperature and precipitation affect water and carbon fluxes in an Asian tropical rainforest, using a combination of field measurements, simplified hydrological and carbon models, and Global Climate Model (GCM) projections. The model links the canopy photosynthetic flux with transpiration via a bulk canopy conductance and semi-empirical models of intercellular CO_2 concentration, with the transpiration rate determined from a hydrologic balance model. The primary forcing to the hydrologic model are current and projected rainfall statistics. A main novelty in this analysis is that the effect of increased air temperature on vapor pressure deficit (D) and the effects of shifts in precipitation statistics on net radiation are explicitly considered. The model is validated against field measurements conducted in a tropical rainforest in Sarawak, Malaysia under current climate conditions. On the basis of this model and projected shifts in climatic statistics by GCM, we compute the probability distribution of soil moisture and other hydrologic fluxes. Regardless of projected and computed shifts in soil moisture, radiation and mean air temperature, transpiration was not appreciably altered. Despite increases in atmospheric CO_2 concentration (C_a) and unchanged transpiration, canopy photosynthesis does not significantly increase if C_i/C_a is assumed constant independent of D (where C_i is the bulk canopy intercellular CO_2 concentration). However, photosynthesis increased by a factor of 1.5 if C_i/C_a decreased linearly with D as derived from Leuning stomatal conductance formulation [R. Leuning. Plant Cell Environ 1995;18:339–55]. How elevated atmospheric CO_2 alters the relationship between C_i/C_a and D needs to be further investigated under elevated atmospheric CO_2 given its consequence on photosynthesis (and concomitant carbon sink) projections.

Keywords: Elevated CO_2; Stochastic processes; Water balance; Tropical rainforest; Photosynthesis; Transpiration

1. Introduction

The projected growth in atmospheric greenhouse gases within the coming century, as summarized by the Intergovernmental Panel on Climate Change report (e.g., [19]), will significantly impact global and regional

* Corresponding author. Fax: +81 983 38 1004.
E-mail addresses: kuma@forest.kyushu-u.ac.jp (T. Kumagai), gaby@duke.edu (G.G. Katul), amilcare@duke.edu (A. Porporato), saitoh@forest.kyushu-u.ac.jp (T.M. Saitoh), mizue.ohashi@joensuu.fi (M. Ohashi), t_ichie@yahoo.co.jp (T. Ichie), suzuki@fr.a.u-tokyo.ac.jp (M. Suzuki).

0309-1708/$ - see front matter © 2004 Elsevier Ltd. All rights reserved.
doi:10.1016/j.advwatres.2004.10.002

Nomenclature

A	daily canopy photosynthetic rate (mol m^{-2} d^{-1})
a, b	constant physiological parameters describing the dependence of C_i/C_a on D
C_a	ambient CO_2 concentration (ppmv)
C_i	bulk canopy intercellular CO_2 concentration (ppmv)
D	vapor pressure deficit (kPa)
d_{season}	number of days in each season (day)
$e_{sat}(T'_a)$	saturation vapor pressure at T'_a (kPa)
f	limiting factor related to a transpiration plateau at high D
$f_T(\tau)$	probability density function of τ
$f_H(h)$	probability density function of h
h	amount of rainfall when rainfall occurs (mm)
I_c	interception (mm d^{-1})
K_s	saturated hydraulic conductivity (mm d^{-1})
L	latent heat of vaporization of water (J kg^{-1})
P	precipitation (mm d^{-1})
p_a	atmospheric pressure (kPa)
P_{season}	total amount of rainfall for each season (mm)
Q	leakage loss (mm d^{-1})
R_{ag}	above-ground biomass respiration (μmol m^{-2} s^{-1})
R_C	constant parameter
R_{eco}	daytime ecosystem respiration (μmol m^{-2} s^{-1})
RH	relative humidity (dimensionless)
R_s	solar radiation (W m^{-2})
R_{soil}	daytime average soil respiration (μmol m^{-2} s^{-1})
R_n	net radiation (W m^{-2})
R'_n	daily average net radiation (W m^{-2})
s	volumetric soil moisture content averaged over the 0–50 cm soil layer (mm)
t	time (day)
T'_a	daytime average air temperature (°C)
T_r	transpiration (mm d^{-1})
WUE	water use efficiency (μmolCO_2 $mmol^{-1}H_2O$)
α	Priestley–Taylor coefficient
β	constant parameter
γ	psychrometric constant (Pa K^{-1})
Δ	rate of change of saturation water vapor pressure with temperature (Pa K^{-1})
η	mean depth of rainfall events (mm)
Θ	relative extractable water in the soil (m^3 m^{-3})
κ_1, κ_2, κ_3	unit conversion factors
$1/\lambda$	mean interval time between rainfall events (day)
ρ_w	density of water (kg m^{-3})
τ	interval between rainfall events (day)

temperatures with concomitant modifications to precipitation patterns. Tropical rainforests are among the most important biomes in terms of annual primary productivity and water cycling; hence, assessing their sensitivity to potential shifts in global and regional temperatures and precipitation patterns is a necessary first step to quantifying future local, regional, and global carbon and water cycling. Although these forests now cover only 12% of the total land surface [10], they contain about 40% of the carbon in the terrestrial biosphere [63] and are responsible for about 50% of terrestrial gross primary productivity [13]. Also, tropical rainforests are a major source of global land surface evaporation [5] with profound influences on both global and regional climate and hydrological cycling (e.g., [31,45]). This large latent energy fluxes from tropical rainforests is known to influence global atmospheric circulation patterns [50].

Although tropical forests in Southeast Asia are about 17% of the total tropical rainforest area [10], relative deforestation rates [38] and estimated resulting CO_2 emissions [20,38] are highest in this region. These forests remain a viable resource for the economies of several Southeast Asian countries such as Malaysia, yet their potential as a carbon sink received much less attention than those of Amazonian rainforests (e.g., [9,12,14,17,35,39,40,62,64,65]).

What is also lacking is an understanding of how hydrologic changes in future climates might impact the carbon cycling in these tropical rainforests, the subject of this investigation. Climate of the maritime environments in Southeast Asian tropics is quite different from those of environments of South American and Central African tropics. While there are clearly periodic dry periods in South American and Central African tropics, maritime Southeast Asian tropics do not have phase-locked dry period [29] because this climatic condition is formed by a combination of a summer monsoon from the Indian Ocean, a winter monsoon from the Pacific Ocean and the South China Sea, and Madden and Julian Oscillation (MJO). As a result, the solar radiation and the air temperature have small seasonal variations and the annual rainfall is evenly distributed throughout the year [22,29]. However, there are some unpredictable intra-annual dry spells [28] and inter-annual dry sequences [27] that may intensify in future climate.

Intra-annual dry spells, in particular, occur every year and often throughout the year.

Our goal is to investigate how carbon and water cycling of a lowland dipterocarp forest in Southeast Asian humid tropics will respond to current and projected atmospheric CO_2 concentration and climate (i.e., air temperature and precipitation patterns). This work builds on an earlier study that investigated how the hydrologic budgets are altered by projected shifts in precipitation only using field measurements, Global Climate Model (GCM) simulation output, and a simplified hydrologic model [26]. In the present study, we go further and use these GCM simulation outputs of current and future air temperature and precipitation statistics, projected atmospheric CO_2 concentration, a carbon flux model [24] combined with a simplified hydrological model described in [54,30,52], and field measurements conducted over a 2-year period to address the study goals. Prior to assessing the carbon and water budget for future climate scenarios, the model is first validated with field measurements conducted in a tropical rainforest in Lambir Hills National Park, Sarawak, Malaysia, over a 2-year period, described next.

2. Study site and measurements

While much of the site and instrument description relevant to the hydrologic cycle are presented in [26], a review and description of the carbon flux measurements are provided for completeness.

2.1. Site description

The experiment was carried out in a natural forest in Lambir Hills National Park (4°12′N, 114°02′E), 30 km south of Miri City, Sarawak, Malaysia (Fig. 1). A 4 ha experimental plot at an altitude of 200 m and on a gentle slope (<5°) was used in this project. An 80-m-tall canopy crane with a 75-m-length rotating jib was constructed in the center of this plot to provide access to the upper canopy. Observational stage at 59.0 m high was devoted to eddy-covariance flux measurements. The canopy height surrounding the crane is about 40 m but the height of emergent treetops can reach up to 50 m.

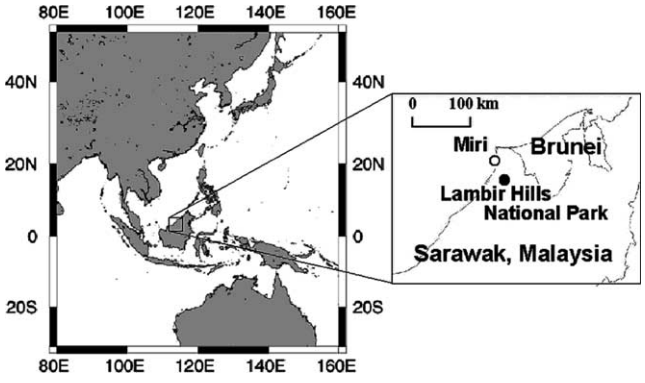

Fig. 1. Location of Lambir Hills National Park, Sarawak, Malaysia.

The mean annual rainfall at Miri Airport (4°19′N, 113°59′E), 20 km from the study site, for the period 1968–2001 was around 2740 mm with some seasonal variation. For example, the mean rainfall for September–October–November (SON) was around 880 mm and for March–April–May (MAM) was around 520 mm. The mean annual temperature is around 27 °C with little seasonal variation (e.g., [29]).

The rain forest in this park consists of two types of native vegetation common to *the whole Borneo*, i.e., mixed dipterocarp forest and tropical heath forest [68]. The former contains various types of dipterocarp trees, which cover 85% of the total park area. The soils consist of red–yellow podzonic soils (Malaysian classification) or ultisols (USDA Soil Texonomy), with a high sand content (62–72%), an accumulation of nutrient content at the surface horizon, a low pH (4.0–4.3), and a high porosity (54–68%) [23,56].

The leaf area index (LAI) was measured in 2002 using a pair of plant canopy analyzers (LAI-2000, Li-Cor, Lincoln, NE) every 5 m on a 30×30 m^2 subplot. The LAI ranged from 4.8 to 6.8 m^2 m^{-2} with a mean of 6.2 m^2 m^{-2} [28]. The amount of monthly litter-fall was evenly distributed throughout the year suggesting minor variations in LAI.

2.2. Micrometeorological and soil moisture measurements

The following instruments were installed at the top of the crane, 85.8 m from the forest floor: a solar radiometer (MS401, EKO, Tokyo, Japan), an infrared radiometer (Model PIR, Epply, Newport, RI), and a tipping bucket rain gauge (RS102, Ogasawara Keiki, Tokyo, Japan). At a separate tower located some 100 m south from the crane, the upward short-wave radiation and long-wave radiation were measured using a solar radiometer (CM06E, Kipp & Zonen, Delft, Netherlands) and an infrared radiometer (Model PIR, Epply, Newport, RI) installed upside down since December 15, 2001. Samples for radiation were taken every 5 s and an averaging period of 10 min was used (CR10X datalogger, Campbell Scientific, Logan, UT). These measurements were used to compute net radiation (R_n; W m^{-2}). Maximum and average total daily solar radiation was 24.5 and 16.7 MJ m^{-2} d^{-1}, respectively, and maximum and average total daily net radiation was 18.2 and 11.5 MJ m^{-2} d^{-1}, respectively.

At the subplot for the in-canopy microclimate measurements, we sampled mean air temperature and humidity at heights of 41.5, 31.5, 21.5, 11.5, 6.5 and 1.5

m using a series of ventilated sensors with dataloggers (H0803208 and RS1, Onset, Pocasset, MA) at 10-min intervals.

Volumetric soil moisture content and matric potential were measured in a subplot at 10, 20 and 50 cm below the forest floor using TDR (CS615, Campbell Scientific, Logan, UT) and tensiometer (DIK3150, Daiki, Tokyo, Japan) at 10-min intervals (CR23X datalogger, Campbell Scientific, Logan, UT). The relative extractable water in the soil (Θ; $m^3\ m^{-3}$) and the soil moisture content over the 0–50 cm soil layer (s; mm) were computed as described in [26].

2.3. Flux measurements

A three-dimensional sonic anemometer (DA-600, Kaijo, Tokyo, Japan) was installed at 60.2 m, i.e., 20 m above the mean canopy height. Co-located with the sonic anemometer is an open-path CO_2/H_2O analyzer (LI-7500, Li-Cor, Lincoln, NE) placed about 30 cm away. Wind speeds and gas concentration time series were all sampled at 10 Hz. All variances and covariances required for eddy-covariance flux estimates were computed over a 30-min averaging interval using the procedure described in [28].

The CO_2 concentration profile measurement within canopy was carried out about 70 m from the crane. Air samples were drawn at 1.5, 6.5, 11.5, 21.5, 31.5 and 41.5 m above ground level using diaphragm pumps and an auto solenoid switching system, and the CO_2 concentration was measured using a closed-path CO_2 infrared gas analyzer (LI-800, Li-Cor, Lincoln, NE). The CO_2 channels were automatically calibrated everyday using a N_2 gas and a 510 ppmv CO_2 standard gas and all raw data were recorded (CR10X datalogger, Campbell Scientific, Logan, UT).

The soil CO_2 efflux was measured manually in 2002 (DOY 134–137, 234–235, 306–308 and 341–343) using a portable IRGA (LI-6400, Li-Cor, Lincoln, NE) connected to a chamber (6400-09 soil CO_2 flux chamber, Li-Cor, Lincoln, NE) at 25 points every 10 m on the $40 \times 40\ m^2$ subplot. The soil CO_2 efflux data were averaged over the subplot for each measurement day, and were regarded as the daytime average values of the soil respiration rate. As there were small variations in soil temperature at a depth of 2 cm during the measurement period (25–28 °C), the dependency of daytime average soil respiration (R_{soil}) on temperature could not be discerned. Moreover, the relationship between R_{soil} and soil moisture was not significant. Thus, daytime R_{soil} was regarded as a constant 5.73 μmol $m^{-2}\ s^{-1}$, computed by averaging the daytime R_{soil}.

To obtain evaporative flux from a wet canopy, a plot representative of the 4 ha experimental plot was instrumented for throughfall and stemflow measurements. Details on throughfall and stemflow measurements are presented in [41,26].

2.4. Derivation of canopy transpiration and photosynthetic rate

Canopy transpiration rate can be obtained as above-canopy H_2O flux when the canopy was dry. Net ecosystem CO_2 exchange (NEE) was derived as the sum of the above-canopy CO_2 flux, which is obtained using the eddy covariance system above the canopy, and the within-canopy storage flux, which is determined by quantifying the rate of change of the CO_2 concentration of the air column within the canopy. Maximum and average daily transpiration rates during the measurement period were 5.09 and 2.52 mm d^{-1}, respectively, and daytime average NEE and its maximum value were −7.06 and −12.74 μmol $m^{-2}\ s^{-1}$, respectively (negative values denote net ecosystem CO_2 uptake).

Power system failure and exclusion of unreliable data limited the amount of runs collected from the flux measurement system. Available data of the above-canopy CO_2/H_2O fluxes and the NEE were 41% and 30% of the total possible period between June 15, 2001 and November 15, 2002, respectively. We filled data gaps and replaced unreliable data (e.g., data obtained when rainfall occurred) using the light-response curve (Saitoh et al., unpublished data) and according to Kumagai et al. [29]. In addition, we obtained the daytime ecosystem respiration (R_{eco}) from the intercept of the light-response curve (average daytime R_{eco}; 8.83 μmol $m^{-2}\ s^{-1}$) and then proceeded to derive a relationship between the daytime R_{eco} and Θ as given by (Saitoh et al., unpublished data): 0.36 mol $m^{-2}\ d^{-1}$ ($0 \leqslant \Theta < 0.5$) and 0.42 mol $m^{-2}\ d^{-1}$ ($0.5 \leqslant \Theta \leqslant 1.0$).

At this site no above-ground biomass respiration (R_{ag}) measurements were collected, and we used a daily average R_{ag} of 1.9 μmol $m^{-2}\ s^{-1}$ estimated using the functional model for tropical rainforest woody tissue respiration [42] and assuming that wood respiration is nearly equal to leaf respiration [37]. The daytime R_{eco} expressed as $R_{soil} + R_{ag}$ was 7.6 μmol $m^{-2}\ s^{-1}$. Taking uncertainties in estimating R_{ag} into account, daytime R_{eco} obtained from the result of eddy-covariance flux measurement (i.e., the light response curve) and from $R_{soil} + R_{ag}$ is sufficiently close. Hence, we concluded the R_{eco} from the eddy-covariance flux measurement is representative of ecosystem-scale values. As a result, canopy photosynthetic rate can be obtained by subtracting the daytime R_{eco} from the daytime NEE (note that negative values denote net ecosystem CO_2 uptake).

While precipitation, solar radiation, and air temperature have small seasonal variations, intra-annual dry spells have been reported [28]. As the intra-annual dry spells often occur throughout the year, transpiration rate is likely to be overly sensitive to the soil moisture condition.

3. Methodology

We discuss first the carbon and water cycling model, as well as its parameterization and testing for this experiment, and then proceed to discuss its usage for assessing shifts in the carbon and water vapor fluxes following projected increases in atmospheric CO_2 concentration and concomitant shifts in climatic factors such as precipitation, air temperature and humidity and net radiation. For the model testing, climatic factors time series were measured and used to drive the model calculations; however, in our model simulations for future climates, only precipitation statistics and potential increment in atmospheric CO_2 concentration and temperature were available thereby necessitating a stochastic treatment. The generation of stochastic precipitation and the other climatic factors time series, and the connections to GCM simulation outputs are also discussed.

The structure of the carbon and water cycling model is schematically shown in Fig. 2a, illustrating all the linkages between meteorological inputs and model outputs.

3.1. Carbon flux modeling

The daily canopy photosynthetic rate A (mol m^{-2} d^{-1}) can be obtained from the water use efficiency (WUE; μmolCO_2 $mmol^{-1}H_2O$) and the daily transpiration rate (T_r; mm d^{-1}) using [24]

$$A = \mathrm{WUE} \cdot \kappa_1 T_r \tag{1}$$

in which

$$\mathrm{WUE} = \frac{C_a\left(1 - \frac{C_i}{C_a}\right)}{1.6\kappa_2 D}, \tag{2}$$

where C_a and C_i are the ambient and the bulk canopy intercellular CO_2 concentration (ppmv), respectively, and D is the vapor pressure deficit (kPa). κ_1 and κ_2 are unit adjustment coefficients (5.56×10^4 mmol m^{-2} mm^{-1} and 9.87 mmol mol^{-1} kPa^{-1}, respectively). The sign convention for photosynthesis is that CO_2 uptake by plants is positive. With T_r predicted from a model (described later) using environmental variables and projected C_a, Eqs. (1) and (2) cannot predict A because C_i remains unknown. Hence, additional equations relating C_i to other known quantities are required. For simplicity, we tested two models for C_i:

$$\frac{C_i}{C_a} = R_C \tag{3}$$

and

$$\frac{C_i}{C_a} = a - bD, \tag{4}$$

where R_C, a and b are constant parameters. That is, C_i/C_a is assumed constant for a wide range of environmental conditions (the Norman model; [46,66]) in Eq. (3) and is sensitive to D (the Leuning model; [24,33]) in Eq. (4). We chose these two models because they optimally reproduced porometry and stable-isotope measured C_i/C_a for ambient and enriched CO_2 conditions over a 3-year period at the Free Air CO_2 Enrichment (FACE) experiments conducted in a maturing pine forest, in Durham, NC, USA [24]. A review of the Norman and the Leuning models is in Appendix A.

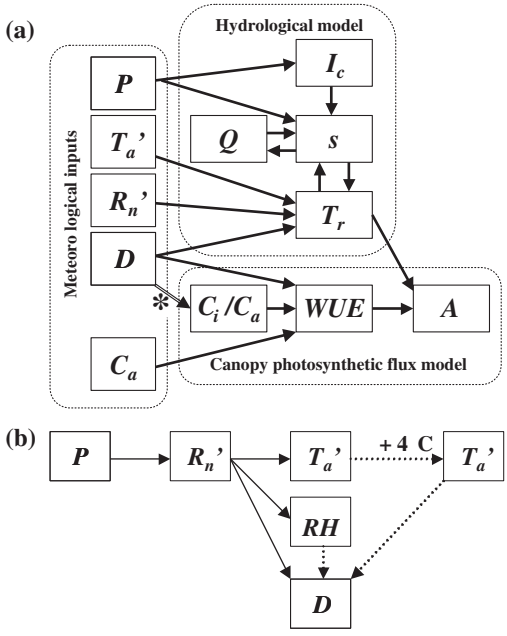

Fig. 2. Schematic diagram of the model framework: (a) inputs, operations, and outputs of carbon and water cycling, and (b) procedures for determining the climatic factors from precipitation. Asterisk represents the C_i/C_a determined by the Leuning model (see Eq. (4)). Dotted arrow represents the procedures for future climatic scenarios.

With predicted T_r from the hydrologic model (see next section) and measured C_a, the parameters R_C, a and b were estimated using non-linear least-squares regression between modeled and eddy-covariance observed A. Based on our regression analysis, we obtained R_C of 0.88, a of 0.99 and b of 0.20. These values are reasonable for "canopy-scale surface" C_i/C_a calculated from the relationship between maximum surface CO_2 assimilation rate and maximum surface conductance for a wide range of vegetation types (see Fig. 3C in [60]). Also, as discussed in [24], a must be unity, a fact that is independently reproduced by our optimization.

3.2. The hydrologic model

As evidenced from the above derivation, predicting T_r is crucial for computing A. Much of the hydrologic model derivation, which was used to predict T_r, was presented in [26]; however, for completeness, we briefly recall here the relevant equations and assumptions.

For gentle slopes, where lateral movement can be neglected, the vertically integrated continuity equation is given by

$$\frac{ds}{dt} = P - T_r - I_c - Q, \tag{5}$$

where s is the volumetric soil moisture content averaged over the root zone (mm), t is the time (day), P is the precipitation (mm d^{-1}), T_r is, as before, the transpiration (mm d^{-1}), I_c is the interception (mm d^{-1}) and Q is the leakage loss (mm d^{-1}) from the soil layer. Given that the root zone is shallow, we assume that the top 50 cm soil layer captures much of the root zone water uptake activity. Also, we assume that Q includes runoff, and that soil evaporation is insignificant when compared to the total transpiration flux (given the high LAI at the site, this assumption is reasonable) (e.g., [25]). The parameterizations of T_r, I_c, and Q for the site are described next.

3.3. Transpiration modeling

The primary forcing variable for transpiration in the tropics is net available energy. Hence, we use a modified Priestley and Taylor [53] expression to compute daily transpiration rate T_r (mmday^{-1}) given by

$$T_r = \kappa_3 f \alpha \frac{\Delta}{L\rho_w(\Delta+\gamma)} R'_n, \tag{6}$$

where α is the Priestley–Taylor coefficient, Δ is the rate of change of saturation water vapor pressure with temperature (Pa K^{-1}), L is the latent heat of vaporization of water (J kg^{-1}), ρ_w is the density of water (1000 kg m^{-3}), γ is the psychrometric constant (66.5 Pa K^{-1}), and R'_n is the daily net radiation above the canopy (W m^{-2}). κ_3 is a unit conversion factor (8.64×10^7 mm s m^{-1} d^{-1}). Thermodynamic variables Δ and L are calculated based on mean air temperature averaged over daylight hours. Daily net radiation was obtained by averaging hourly values. In Eq. (6), f is the limiting factor related to a transpiration plateau at high D (e.g., [43]). Using a function for stomatal response to increasing D from [48,49], we assume a simplified form f given by

$$f = \begin{cases} 1 & \text{for } D < 1, \\ 1 - 0.6\ln D & \text{for } D \geqslant 1. \end{cases} \tag{7}$$

The model formulation in [48,49] was shown to be reasonably accurate for a wide range of ecosystem types and D ranges. A major uncertainty in the transpiration model is which, for forested ecosystems, is usually less than its typical 1.26 value because of additional boundary layer, leaf, xylem, and root resistances. We conducted a detailed sensitivity analysis in [26] and demonstrated that the best estimator of α is

$$\alpha = 0.49\Theta + 0.52 \quad \text{for } 0 \leqslant \Theta \leqslant 1.0. \tag{8}$$

3.4. Interception modeling

In [26], the relationships between daily rainfall P, throughfall TF and stemflow SF were described as linear regression equations, and daily interception I_c was related to P after subtracting both TF and SF from P to give

$$I_c = \begin{cases} P & \text{for } 0 \leqslant P < 0.90, \\ 0.13P + 0.78 & \text{for } 0.90 \leqslant P < 3.91, \\ 0.084P + 0.96 & \text{for } 3.91 \leqslant P. \end{cases} \tag{9}$$

3.5. Leakage losses modeling

In [26], the leakage loss rate (Q) was parameterized using

$$Q = K_s \Theta^{\beta}, \tag{10}$$

where K_s is the saturated hydraulic conductivity (mm d^{-1}) and β the fitted parameter. The parameters K_s and β were estimated using non-linear least-squares regression between s calculated from Eq. (5) and observed s. Based on our regression analysis, we obtained a K_s of 33.4, typical for loam and sandy loam, and β of 5.3, typical for wet sandy clay loam and dry clay [4]. The minor differences between K_s and β computed here and those reported in [26] are strictly due to the differences in the T_r model.

Details on the ponding and infiltration calculations are discussed in [26]. When testing the model, measured time series of the climatic factors (precipitation, radiation, temperature, humidity and CO_2) are used to drive the calculations. However, for future climate simulations, synthetic climatic drivers time series must be constructed as described next.

3.6. Simulations of precipitation

Current and future climatic factors time series were constructed using relationships between precipitation and other climatic factors obtained in the 2001–2002 observation period, rainfall records collected in 1968–2001 and GCM outputs for air temperature and precipitation for 2070–2100 (details described later). As a result, current and future time series (i.e., the 1968–2001 and the 2070–2100) of each hydrological component and carbon flow at the site can be computed. From the simulated time series of each hydrological components and carbon flow, their statistics for the period 1968–2001 and 2070 can then be calculated. We then examine shifts in the statistics of these hydrological components and carbon flows based on these anticipated changes in the climatic (or forcing) factors.

It is necessary to first construct the rainfall time series because they are needed for constructing other climatic

factors. Current and future rainfall time series (i.e., the 1968–2001 and the 2070–2100) were constructed as the series of random numbers generated according to probability distributions representing the 1968–2001 and the 2070–2100 rainfall characteristics at the site. As discussed in [26], we assumed the frequency and amounts of rainfall events to be stochastic variables, in which interval between precipitation events, τ (day), is expressed as a exponential distribution given by

$$f_T(\tau) = \lambda \exp(-\lambda\tau) \quad \text{for } \tau \geqslant 0, \tag{11}$$

where $1/\lambda$ is the mean interval time between rainfall events (day). The amount of rainfall when rainfall occurs, h (mm), is also assumed to be an independent random variable, expressed by an exponential probability density function [30]:

$$f_H(h) = \frac{1}{\eta} \exp\left(-\frac{1}{\eta}h\right) \quad \text{for } h \geqslant 0, \tag{12}$$

where η is the mean depth of rainfall events (mm).

For the 1968–2001 rainfall scenario, a long-term data record obtained at Miri Airport was used to assess the descriptive skill of the above precipitation model. For the 2070–2100 rainfall scenarios, a number of transient climate GCM simulations from the Hadley Centre for Climate Prediction and Research, available through a public website, were used. The 2070–2100 time series of climatic factors at coordinates (2°30′–5°N, 112°30′–116°15′E) was constructed from the HadCM3 run (e.g., [11]). The Hadley Centre offers climate change predictions formulated as differences between current climate, conventionally defined as 1960–1990, and the climate at the end of the 21st century, taken to be 2070–2100. As in [26], we used average precipitation changes in the period 2070–2100 for each of the four seasons December–February (DJF), March–May (MAM), June–August (JJA) and September–November (SON) and obtained average rainfall in periods 1968–2001 and 2070–2100, respectively, for each season (Table 1). The Hadley Centre projected precipitation shifts for this region (i.e., comparing the climate in 1960–1990 with the climate in 2070–2100) are drier DJF (~180 mm), little change in MAM (~20 mm), wetter JJA (~70 mm), and wetter SON (~140 mm). Parameters $1/\lambda$ and η in 2070–2100 were obtained, using the total amount of rainfall P_{season} (mm) for each season using

$$P_{season} = d_{season}\eta\lambda, \tag{13}$$

where d_{season} is the number of days in each season (day).

We constructed three types of rainfall scenarios for 2070–2100 (Table 1). Rainfall scenario 2070–2100 A, which computes $1/\lambda$ for the 2070–2100 precipitation, but retains η for 1968–2001. Rainfall scenario 2070–2100 B, which computes η for 2070–2100, but retains $1/\lambda$ as in 1968–2001. That is scenarios 2070–2100 A and B assume that future changes in rainfall are caused entirely by changes in rainfall frequency or rainfall depth. In reality, changes in precipitation are due to both frequency and depth. For simulation purposes, it is more constructive to evaluate these two "end members" as agents causing precipitation shifts by assigning the entire shift to be either frequency or depth. To ensure that "no surprises" exist at some intermediate state, we also constructed a rainfall scenario 2070–2100 C as the "intermediate" scenario between these two end members, which computes $1/\lambda$ and η as mean values between in 1968–2001 and in 2070–2100 A and B, respectively.

We assumed that a single storm event does not exceed a day, and that plural storm events during a day can be

Table 1
Rainfall parameters for all scenarios[a]

		DJF	MAM	JJA	SON
2001–2002[b]	Average rainfall (mm/d)	4.92	6.14	6.05	9.73
	$1/\lambda$ (day)	1.76	1.98	2.05	1.42
	η (mm)	8.7	12.0	12.4	13.8
1968–2001[c]	Average rainfall (mm/d)	8.37	5.85	7.70	9.72
	$1/\lambda$ (day)	1.73	2.12	1.82	1.57
	η (mm)	14.5	12.0	14.1	15.3
2070–2100[d]	Average rainfall (mm/d)	6.37	5.65	8.45	11.22
A[e]	$1/\lambda$ (day)	2.28	2.12	1.67	1.36
B[f]	η (mm)	10.9	12.1	15.6	17.6
C	$1/\lambda$ (day)	2.00	2.12	1.74	1.47
	η (mm)	12.8	12.0	14.7	16.5

[a] See Eqs. (11) and (12). DJF, December–January–February; MAM, March–April–May; JJA, June–July–August; SON, September–October–November.
[b] The measurement period September 1, 2001 to August 31, 2002. Average annual rainfall is 2449.5 mm.
[c] Average annual rainfall is 2884.4 mm.
[d] Average annual rainfall is 2888.5 mm.
[e] Values of η are the same as in the 1968–2001 scenario.
[f] Values of $1/\lambda$ are the same as in the 1968–2001 scenario.

lumped together as a single daily storm. Such a simplifying assumption may be reasonable here because single storm events exceeding one day seldom occur at least in the historical record at Miri Airport.

3.7. Current climatic scenario

The current atmospheric CO_2 concentration (i.e., the 1968–2001) was assumed to be 360 ppmv. From the 2001–2002 observation results, we obtained relationships between precipitation, P, and the other climatic factors as follows (see Fig. 2b): (1) In [26], R'_n was related to P via Gaussian random variables with parameters (mean, μ, and standard deviation, σ) that vary with P, that is, $0 \leqslant P < 10$ ($\mu = 145.0$, $\sigma = 33.7$), $10 \leqslant P < 20$ ($\mu = 108.8$, $\sigma = 4.8$) and $20 \leqslant P$ ($\mu = 92.3$, $\sigma = 22.4$). (2) Daytime average air temperature, T'_a (°C), and relative humidity, RH, were related to R'_n through linear regression models [$T'_a = 0.0239R'_n + 23.48$ ($R^2 = 0.65$) and $\mathrm{RH} = -0.0015R'_n + 1.0$ ($R^2 = 0.70$), respectively]. (3) An exponential model was fitted to related D to R'_n ($D = 0.112\exp(0.0118R'_n)$, $R^2 = 0.75$). Using the above relationships between P and other climatic factors and the 1968–2001 rainfall scenario, the 1968–2001 climatic factors time series was constructed.

3.8. Future climatic scenarios

The HadCM3 run assumes that future emissions of greenhouse gases will follow the IPCC-IS92a scenario [18], in which the atmospheric concentration of CO_2 increases by about 1% per year. According to the IPCC-IS92a scenario, the atmospheric CO_2 concentrations in 2070 and 2100 are 579.2 and 711.7 ppmv, respectively. Hence, we assumed the 2070–2100 atmospheric CO_2 concentration to be 645 ppmv, a mean value between in 2070 and 2100.

Comparing the climate in 1960–1990 with the climate in 2070–2100 for this region, the Hadley Centre projected that surface air temperature increases by 4 °C for all of the four seasons DJF, MAM, JJA and SON. The warmer climate experiments using a wide variety of GCMs suggest that unchanged relative humidity is realistic [1,21,61,69]. Hence, the modified climate in 2070–2100 might consist of an attendant increase in atmospheric water vapor concentration but roughly retains its relative humidity as in 1960–1990.

For the 2070–2100 scenarios, we determined the climatic factors, such as R'_n, T'_a and D by following procedures (see Fig. 2b): (1) From the 2070–2100 A, B and C rainfall scenarios, R'_n was estimated using the same method (i.e., the Gaussian random numbers generation) as when R'_n in the 1968–2001 climatic scenario was determined. (2) From this estimates of R'_n, T'_a was initially estimated using the relationship between T'_a and R'_n derived from the 2001–2002 observations. Also, RH was estimated using the relationship between RH and R'_n (though the change in RH was minor). (3) In order to obtain elevated regional air temperature, new estimates of T'_a were made by adding 4 °C to the initial estimates of T'_a. (4) From $D = e_{sat}(T'_a)(1 - \mathrm{RH})$ (where $e_{sat}(T'_a)$ is the saturation vapor pressure at T'_a, in kPa), D under the condition of air temperature increase was computed.

As a result, we obtained the 2070–2100 A, B and C scenarios as future climatic scenarios. Before discussing future carbon and water cycling simulations we evaluate the predictive skills of the simplified carbon and water cycling model next.

4. Model results

4.1. Model evaluation

Fig. 3 compares calculated cumulative T_r (ΣT_r) and A (ΣA) against measurements for June 15, 2001 to November 15, 2002. The model well reproduces measured ΣT_r and ΣA despite all the simplifying assumptions. Calculated ΣT_r at the end of the observation period was only 4% higher than the observed value (Fig. 3a). While cal-

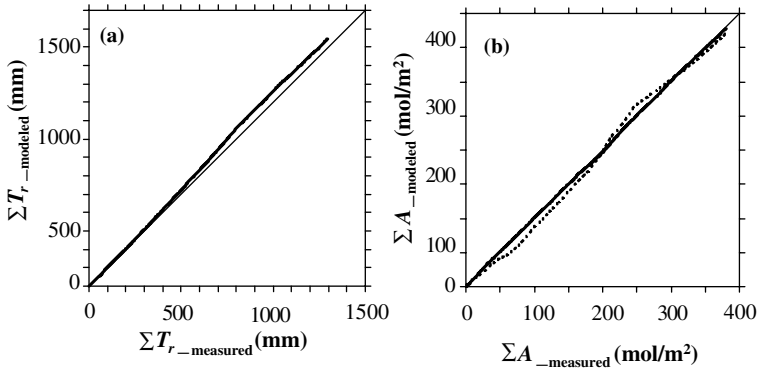

Fig. 3. Comparisons between measured and modeled (a) cumulative transpiration rate and (b) cumulative photosynthetic rate (dotted line; the Norman model, solid line; the Leuning model) for June 15, 2001 to November 15, 2002.

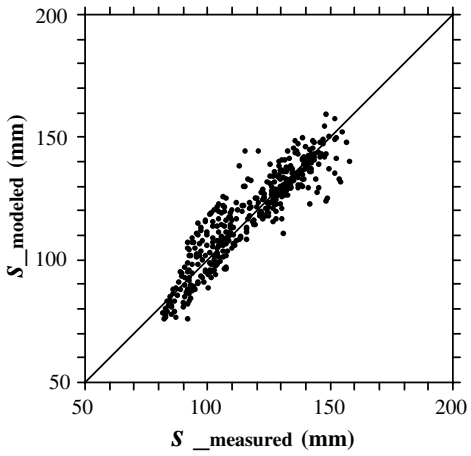

Fig. 4. Comparison between measured and modeled soil moisture.

culated ΣA in the Norman model agreed well with the observed value (within 3%), the slope of calculated ΣA in the Leuning model was not statistically different from unity (Fig. 3b). This suggests that despite the small discrepancies between observed and calculated values in the Norman model, the calculation for A under current climatic conditions is robust to variations in D.

Since the reproduction of s is important because s is fundamental to estimating A through its effect on α and T_r, it is necessary to compare how well the measured and modeled s agree (Fig. 4).

4.2. Carbon and water balances

The model estimated annual T_r and I_c in the measurement period 2001–2002 to be 951.3 and 386.2 mm, respectively, suggesting that I_c can be up to 40% of T_r (Table 2). The ratio of I_c to annual precipitation (P) was 16%. Evapotranspiration, computed as the sum of T_r and I_c, was 1337.5 mm, accounting for about 55% of total P. On the other hand, averaged annual T_r and I_c for the 1968–2001 scenario (hereinafter referred to as 1968) were 998.6 and 408.5 mm, respectively (Table 2). Note that total P in 2001–2002 was about 440 mm less than in 1968 scenario. As a result, evapotranspiration and its ratio to total P in 1968 scenario, which is the "standard" period, were 1407.1 mm and about 49%, respectively. Evapotranspiration studies by Bruijnzeel [3] for humid tropical forests suggests that: (1) annual T_r was, on average, 1045 mm (range 885–1285 mm), (2) I_c was, on average, 13% of incident P (range between 4.5% and 22%), and (3) annual evapotranspiration ranged from 1310 to 1500 mm. Our values for evapotranspiration and interception losses for both 2001–2002 and 1968 scenario are comparable to those reported values. Although the majority of R_n was transformed into latent heat (LE) for both 2001–2002 (78%) and 1968 scenario (82%), LE positively correlated with P (Table 2). Interestingly, most measurements on the fraction of R_n converted to LE = (LE/R_n) reported for other tropical forests did not consider the evaporation from the wet canopy. Our results included wet canopy evaporation in the energy partitioning. When we calculated LE using only T_r, annual averaged LE/R_n in 2001–2002 and 1968 scenario were 0.55 and 0.58, respectively. Our LE/R_n for the dry year (i.e., 2001–2002) and the standard year (i.e., 1968 scenario) correspond to LE/R_n measurements collected during the dry and the transition seasons in the Amazonian tropical forests [40,65], respectively.

There were little changes in annual P between the scenario 1968 and in the future scenarios 2070–2100A, 2070–2100B and 2070–2100C (hereinafter referred to as A, B and C, respectively) thereby in annual I_c, while annual T_r decreased by about 20 mm and annual Q increased by about 30 mm in the future scenarios: some compensation emerged (Table 2). According to Kumagai et al. [26], seasonal shift in each hydrologic component for the future scenarios introduced some cancellation, that is, on annual timescales, all hydrologic components experienced minor changes under projected precipitation scenarios. However, in the future scenarios of this study, owing to a minor decrease in annual T_r caused by an increase in D, annual Q mildly increased. Furthermore, the computed R_n for all the scenarios were comparable. Hence, the year total LE/R_n for future scenarios hardly changed (Table 2). Although some differences in hydrologic components among the future scenarios were observed at seasonal timescales, they dis-

Table 2
Annual water and carbon balance for all scenarios[a]

Scenario	P (mm)	T_r (mm)	I_c (mm)	Q (mm)	R_n (MJ/m^2 d)	LE[b]/R_n	A (tC/ha y)	
							NR[c]	LU[c]
2001–2002	2449.5	951.3	386.2	1041.4	11.50	0.78	33.3	32.3
1968–2001	2884.4	998.6	408.5	1477.5	11.48	0.82	32.4	33.7
2070–2100A	2891.5	975.9	408.1	1507.5	11.50	0.80	36.4	57.3
2070–2100B	2891.5	978.8	408.9	1504.0	11.49	0.81	36.5	57.5
2070–2100C	2891.5	976.4	406.9	1507.9	11.49	0.80	36.4	57.3

[a] See Table 1.
[b] Latent heat flux.
[c] NR, the Norman model; LU, the Leuning model.

appeared at annual timescales (see [26]). An immediate consequence of the computed T_r not significantly changing in all three future climate scenarios is that all the changes in photosynthesis are attributed to changes in WUE, discussed next.

Annual A estimated using the Norman model [46] and the Leuning model [33] for the measurement period 2001–2002 (33.3 and 32.3 tC ha^{-1} y^{-1}, respectively) were not significantly different from those for scenario 1968 (32.4 and 33.7 tC ha^{-1} y^{-1}, respectively) (Table 2). Those values are comparable to the 30.4 tC ha^{-1} y^{-1} reported for an Amazonian tropical rainforest [37]. Annual A in the scenario 1968 calculated using the Norman and the Leuning models were also comparable (Table 2). However, when using the Norman model for the future scenarios a slight increase in annual A was obtained. On the other hand, annual A calculated by the Leuning model markedly increased for the future scenarios (Table 2). For A in the future scenarios computed by the Norman model, marked increases in D reduced WUE thereby eliminating the expected enhancement in WUE attributed to increased C_a. Mathematically, if R_C (≈ 0.88) is constant,

$$\mathrm{WUE} = \frac{C_a(1-R_C)}{1.6\times 9.87D} \approx \frac{C_a}{D}\frac{0.12}{1.6\times 9.87}.$$

In the Leuning model, C_i/C_a linearly decreases with increasing D thereby offsetting the expected reduction in WUE by increased D. Hence, for the Leuning model, WUE was primarily affected by an increase in C_a only. Mathematically, the Leuning model with parameters $a \approx 1$ and $b = 0.2$ leads to a WUE that is independent of D and is given by

$$\mathrm{WUE} = \frac{C_a\{1-(0.99-0.2D)\}}{1.6\times 9.87D} \approx C_a\frac{0.2}{1.6\times 9.87}$$

which linearly increases with increasing C_a.

Again, on annual timescales, the differences in annual A among scenarios A, B and C were negligible.

4.3. Soil moisture

Ensemble seasonal probability distributions of soil moisture content ($p(s)$) for scenarios 1968, A, B and C are compared in Fig. 5. $p(s)$ for the measurement period 2001–2002 is also compared. Note that for SON in scenario 1968 and 2001–2002 which have similar rainfall (see Table 1), $p(s)$ is about the same despite lower s tail in 2001 caused by preceding drought (Fig. 5d). Departures in Fig. 5 for the DJF, JJA and whole year $p(s)$ are primarily due to the frequent droughts in 2001–2002 (i.e., flatter tails) when compared to ensemble record of scenario 1968 (see Table 1).

Decrease in heavy rainfall under scenario B does not affect $p(s)$, while decrease in rainfall frequency increases the dry mode (Fig. 5a). Under the condition of increased rainfall, some cancellations occur—for example, storms with smaller (but more frequent) depths are likely to be intercepted; however, storms with bigger depths (but less frequent) contribute to the drainage. Hence, $p(s)$ appears more robust to future shifts in precipitation when compared to interception or drainage (see [26]).

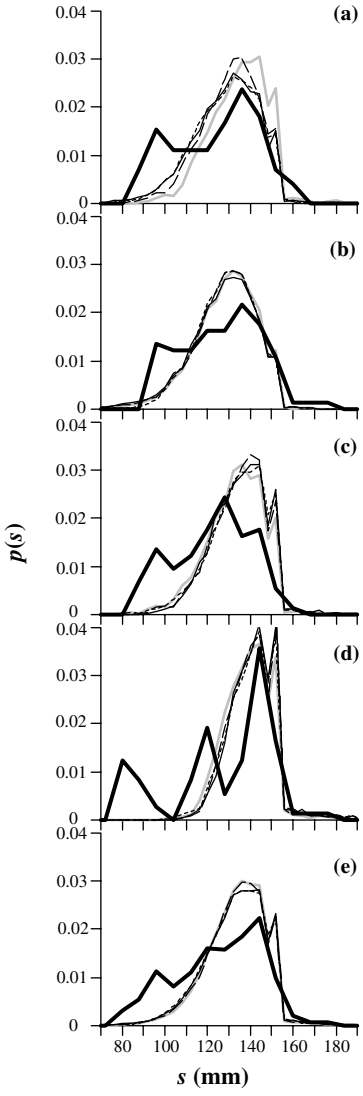

Fig. 5. Modeled probability density functions of soil moisture content ($p(s)$) for the measurement period, September 1, 2001 to August 31, 2002 (thick line) and scenarios 1968–2001 (light solid line), the 2070–2100A (thin solid line), the 2070–2100B (broken line) and the 2070–2100C (dotted line) (see Table 1). (a) DJF, (b) MAM, (c) JJA, (d) SON (see Table 1), and whole year.

4.4. Evapotranspiration

Seasonal cumulative T_r (ΣT_r) and $T_r + I_c$ ($\Sigma(T_r + I_c)$) for the measurement period 2001–2002, current scenario 1968, and future scenarios A, B and C are compared in Fig. 6.

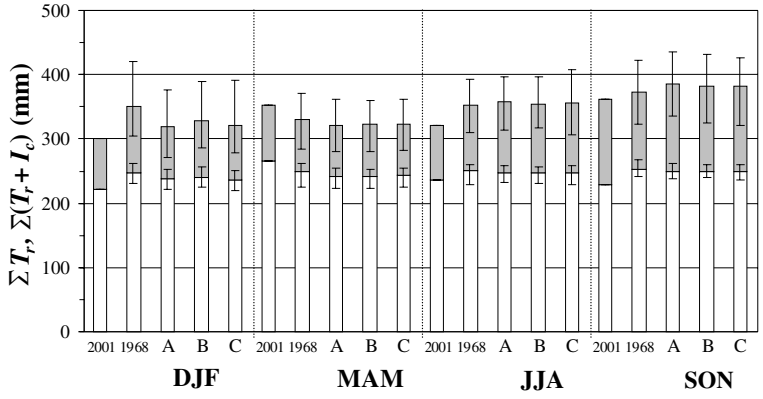

Fig. 6. Cumulative transpiration (ΣT_r) and evapotranspiration rate ($\Sigma(T_r + I_c)$) in each season for the measurement period, September 1, 2001 to August 31, 2002 (2001), scenarios 1968–2001 (1968), the 2070–2100A (A), the 2070–2100B (B) and the 2070–2100C (C) (see Table 1). Blank and shaded columns represent ΣT_r and cumulative interception (ΣI_c), respectively. The top and bottom of the vertical bars in the figure indicate the maximum and minimum values, respectively.

ΣT_r and $\Sigma(T_r + I_c)$ calculated for 2001–2002 were almost within the range of those calculated using 1968 scenario. However, owing to the frequent droughts in 2001–2002, ΣT_r and $\Sigma(T_r + I_c)$ calculated for 2001–2002 were almost identical to the lower values of ΣT_r and $\Sigma(T_r + I_c)$ for scenario 1968 in DJF and JJA (Fig. 6).

For any future scenario, ΣT_r was not appreciably altered in each of the four seasons (Fig. 6).

Decrease in rainfall amount in DJF reduced I_c under the future scenarios A, B and C (Fig. 6). For scenario A, the more frequent light rainfall events were almost perfectly intercepted by the canopy, while under scenario B, the heavier (though less frequent storms) increased I_c (for SON in Fig. 6). For DJF, decreases in I_c determined decreases in $\Sigma(T_r + I_c)$, while for each of the other seasons, $\Sigma(T_r + I_c)$ was not appreciably altered.

4.5. Canopy photosynthesis

Figs. 7 and 8 show seasonal cumulative A (ΣA) for the measurement period 2001–2002 and scenarios 1968, A, B and C, calculated using the Norman and the Leuning models, respectively.

While ΣA calculated by the Leuning model for 2001–2002 was almost within the range of those for scenario 1968 in any season (Fig. 8), in MAM and JJA there were large discrepancies between ΣA calculated by the Norman model for 2001–2002 and for scenario 1968 (Fig. 7). Note that for either model, considering annual ΣA, the discrepancies are reduced because parameter C_i/C_a was determined using yearlong climatic data. Also, on seasonal timescale, using the Leuning model, the discrepancies between ΣA in 2001–2002 and in scenario 1968 were minimized because the C_i/C_a can respond to seasonal variations in D.

For either model, the projected growth in C_a (i.e., 645 ppmv) increased ΣA for all seasons. However, when using the Norman model, ΣA did not increase under future scenarios (Fig. 7). The ΣA calculated by the Leuning model increased up to 170% (Fig. 8). This suggests that for the Norman model (and constant transpiration), an increase in D roughly cancels the increase

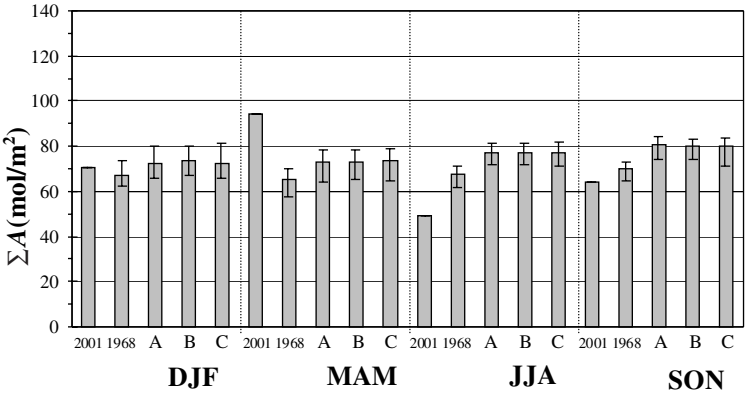

Fig. 7. Cumulative photosynthetic rate calculated using the Norman model ($R_C = 0.88$) for C_i/C_a in each season for the measurement period, September 1, 2001 to August 31, 2002 (2001), scenarios 1968–2001 (1968), the 2070–2100A (A), the 2070–2100B (B) and the 2070–2100C (C) (see Table 1). The top and bottom of the vertical bars in the figure indicate the maximum and minimum, respectively.

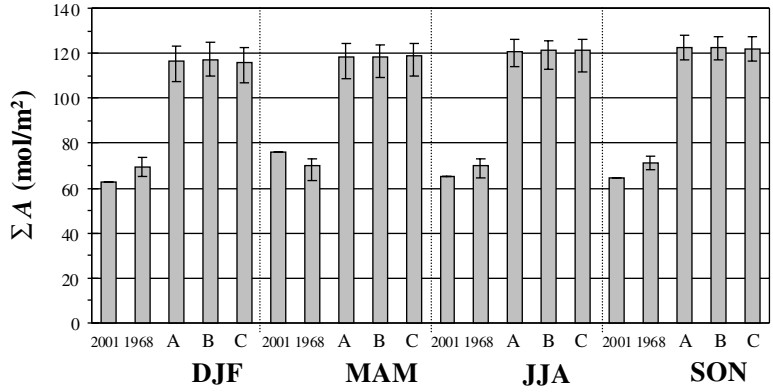

Fig. 8. Same as Fig. 7 but using the Leuning model for C_i/C_a.

Table 3
C_i/C_a for the Norman and the Leuning models, for scenarios 1968–2001, 2070–2100A, 2070–2100B and 2070–2100C

NR[a]	LU[a]			
1968[b], A[c], B and C	1968	A	B	C
0.88	0.87 (0.056)	0.81 (0.059)	0.81 (0.059)	0.81 (0.059)

Standard deviations are shown in parentheses.
[a] NR, the Norman model; LU, the Leuning model.
[b] 1968, 1968–2001 scenario.
[c] A, 2070–2100A scenario; B, 2070–2100B scenario; C, 2070–2100C scenario.

in WUE due to increased C_a thereby resulting in a near-constant ΣA.

The C_i/C_a estimated using the Norman model under all scenarios for A estimates was 0.88 (Table 3). However, using the Leuning model, although the estimated C_i/C_a in scenario 1968 for A were almost the same as values estimated using the Norman model (0.87 ± 0.056), the C_i/C_a in future scenarios A, B and C were significantly reduced (0.81 ± 0.059) because of increases in D (Table 3). As a result, using the Leuning model for future scenarios, increases in ΣA for all season were very large (Fig. 8).

5. Discussion and conclusions

In a previous study [26], how future shifts in precipitation resulting from an increase in global temperature affected water reservoirs and fluxes within an Asian tropical rainforest was examined using a combination of field measurements, simplified water balance models, and GCM projections of precipitation. In the present study, we have examined how the projected increase in atmospheric CO_2 and its concomitant shifts in air temperature, added to shifts in precipitation affect both water fluxes and photosynthesis within an Asian tropical rainforest. We used carbon flux model combined with a simplified hydrological model already developed and tested for this region and GCM projections of air temperature to address the study objective. The field measurements permitted us to derive key relationships for present-day climate that tie the "forcing" term with parameters or state variables. For example, the field data were used to derive relationships between precipitation and variability in net radiation, air temperature and air humidity, between transpiration and extractable water content, between precipitation and interception, the drainage flow parameters, and the parameters for describing C_i/C_a.

The Hadley Centre projected precipitation shifts for this region in 2070–2100 are drier DJF, little change in MAM, wetter JJA, and wetter SON compared to the climate in 1968–2001. We assumed that this shift occurs in one of the two ways: change in precipitation depth or change in precipitation frequency. In reality, both frequency and depth are likely to change; thus, by exploring the "end members" and an "intermediate" precipitation shift scenarios, we can quantify the expected changes in hydrologic fluxes and reservoirs. Based on climate models relative humidity appears invariant to changes in greenhouse warming (e.g., [1,21,61,69]). This invariance in relative humidity, when combined with a 4 °C temperature increase leads to a concomitant increase in water vapor pressure deficit that affects both water use efficiency, and, to a lesser extend transpiration for the site.

The probability distribution of soil moisture ($p(s)$) is sensitive to a decrease in precipitation, in part because smaller depth (but more frequent) precipitation events are efficiently intercepted by the ecosystem. On the other hand, $p(s)$ is robust to an increase in precipitation because larger depth (but less frequent) precipitation events increase primarily the drainage. Regardless of shifts in precipitation (and hence shifts in soil moisture), radiation and mean air temperature, transpiration is not appreciably altered. This lack of sensitivity of transpiration to increases in vapor pressure deficit (D) is due to

the fact that only a D exceeding 1 kPa will reduce stomatal conductance. Despite increases in atmospheric CO_2 concentration and unchanged transpiration, the results for canopy photosynthesis strongly depend on how C_i/C_a will respond to D. In the case of a constant C_i/C_a or even a C_i/C_a that varies with relative humidity (RH) [24] as is the case with the widely used Ball–Berry formulation [6], given by

$$\frac{C_i}{C_a} \approx 1 - \frac{1}{m\,\mathrm{RH}} \tag{14}$$

(where m is the Ball–Berry slope parameter), much of the water use efficiency (WUE) enhancement due to elevated atmospheric CO_2 will be counteracted by the increase in D. The latter increase is attributed to a constant RH and a 4 °C warmer climate. On the other hand, if C_i/C_a linearly varies with D, as is the case for the Leuning model, WUE becomes independent of D and any increase in atmospheric CO_2 results in a proportional increase in WUE and photosynthesis if transpiration is unaltered.

In general, under elevated CO_2, CO_2 uptake of forest canopies is expected to increase as demonstrated by the FACE experiment in a Southeastern United States pine forest (Duke Forest) (e.g., [47,58]). In the Duke Forest FACE experiment with ambient +200 ppm CO_2, the simpler model (i.e., the Norman model) was sufficient for reproducing the photosynthesis rate enhancement through modeling appropriate C_i/C_a [24]. Katul et al. [24] suggested that the CO_2 concentration enhancement is 1.55 and the computed enhancement in photosynthesis from the Norman model is also 1.55. This estimate is in agreement with leaf-level measurements of photosynthesis enhancement by Ellsworth (1.56; [7]). It is important to note that FACE experiments are generally designed to maintain similar microclimatic conditions for ambient and CO_2 enriched conditions; hence, differences between D (or RH) for ambient and enriched plots is minimum. Schäfer et al. [59] showed that for this Duke Forest FACE experiment, D for ambient and enriched plots was similar (see e.g., their Fig. 2). In this study, however, our values of CO_2 uptake estimated using the Norman model under current +300 ppm CO_2 were not much altered when compared to the ambient state mainly because of the ratio of C_a/D was not altered. Furthermore, our values of CO_2 uptake calculated using the Norman and the Leuning models were considerably different, because the Leuning model takes the effect of D into consideration, while the Norman model does not. It is interesting to note that no FACE experiments currently exist that take into consideration increase in D caused by an increase in air temperature attendant on the projected growth in CO_2.

An important consequence of a change in D but constant RH in a future climate scenario is that if the Ball–Berry model [6] was used for computing C_i/C_a, future photosynthesis rate would be similar to those calculated using the Norman model and would not be appreciably altered from their present value. For the Leuning model, photosynthesis increased by a factor of 1.5 when comparing current and future climate. Although the Leuning model is generally regarded as a Ball–Berry type model, this study highlights a fundamental difference between the two approaches. From a physiological point of view, stomata respond to D not RH [49].

Although warmer temperatures could increase rates of all chemical and biochemical processes in plants and soils up to a point where enzymes disintegrate (e.g., [57]), the uncertainty over the interaction between elevated CO_2 and temperature (e.g., [16]) is not small. In general, under elevated CO_2, enhancements of photosynthetic rate are observed (e.g., [7]). However, in a few instances, increasing atmospheric CO_2 has been shown to cause down-regulation of photosynthetic rate (e.g., [15,55]). Preliminary evidence from a FACE experiment in a Southeastern United States hardwood forest suggests that increasing atmospheric CO_2 reduces transpiration rate (e.g., [67]) through a reduction in stomatal conductance (e.g., [36]). Furthermore, increase in atmospheric CO_2 can increase interception by increasing LAI (e.g., [34]).

On much longer time scales, increases in atmospheric CO_2 can induce higher soil water holding capacity because of an increase in soil organic matter content resulting from increased litter production (e.g., [44,59]). In the Duke Forest FACE experiment, however, it is suggested that LAI, stomatal conductance, C_i/C_a and bulk canopy conductance are, to a first order, unaltered by elevated CO_2 [8,24,51,59]. Thus, the effects of elevated CO_2, including its attendant shifts in the other climatic factors, on numerous factors in forest ecosystems still remain uncertain. Further research is now required on the effects of elevated CO_2 on Southeast Asian rainforest ecosystems using extensive and technically difficult experiments.

Acknowledgments

We thank Hua Seng Lee and Lucy Chong for providing the opportunity for this study. This work has been supported by CREST (Core Research for Evolutional Science and Technology) of JST (Japan Science and Technology Agency) and a grant from the Ministry of Education, Science and Culture of Japan (#13760120). We thank Tohru Nakashizuka for his support and the many colleagues who helped us with this work. Tomo'omi Kumagai and Gabriel Katul would like to thank Ram Oren for his useful critique. Gabriel Katul acknowledges support from Duke University's Center on Global Change, the National Science Foundation (NSF-EAR and NSF-DMS), and the Department of

Energy through their Biological and Environmental Research (BER) Program, the Southeast Regional Center (SERC) of the National Institute for Global Environmental Change (NIGEC), and the DOE Terrestrial Carbon Processes Program (TCP) and the FACE project. Amilcare Porporato was supported by the DOE-NIGEC (Great Plains Regional Center) grant DE-FC02-03ER63613.

Appendix A. The Norman and the Leuning models for stomatal conductance

The photosynthetic rate A can be described as

$$A = g_c(C_a - C_i) = g_c C_a\left(1 - \frac{C_i}{C_a}\right), \tag{A.1}$$

where g_c is the stomatal conductance, and C_a and C_i are the ambient and the intercellular CO_2 concentration, respectively.

Wong et al. [66] have shown that the C_i can be approximated by $C_i = 0.80C_a$ for C_3 plants, for a wide range of environmental conditions, but that this relationship varies from species to species. According to Wong et al. [66], Norman [46] assumed that A resulted from changes in which attempt to hold C_i/C_a constant ($= R_C$) for a wide range of environmental conditions (see Eq. (3)).

One widely used g_c model is the Ball–Berry model (see [6]), given by

$$g_c = m\frac{A\,\mathrm{RH}}{C_S} + g_0, \tag{A.2}$$

where m and g_0 are empirical parameters, and RH and C_S are relative humidity and CO_2 concentration at the leaf surface, respectively. Eq. (A.2) is an empirical relationship that incorporates the often-observed correlation between A and g_c, and includes the effects of RH and C_S on g_c. Using Eqs. (A.1) and (A.2) and upon neglecting the leaf boundary layer resistance relative to g_c^{-1} (i.e., $C_a \approx C_S$), a closure model for C_i/C_a, given by Eq. (14), can be derived if g_0 is neglected [24].

However, it is widely accepted that stomata respond to humidity deficit, D, rather than to surface RH (e.g., [2]). Furthermore, since A approaches zero when C_S approaches the CO_2 compensation point, and Eq. (A.2) cannot describe stomatal behavior at low CO_2 concentration [32]. Leuning [32,33] accounted for those observations by replacing RH and C_S in Eq. (A.2) with a vapor pressure deficit correction function $f(D)$ and $C_S - \Gamma$ respectively, i.e.,

$$g_c = m\frac{Af(D)}{C_S - \Gamma} + g_0; \quad f(D) = \left(1 + \frac{D}{D_0}\right)^{-1}, \tag{A.3}$$

where D_0 is the empirical parameter. Using the same approach for deriving a closure model for C_i/C_a described by Eq. (14), the Leuning [33] model reduces to

$$\frac{C_i}{C_a} = 1 - \frac{1}{m}\left(1 - \frac{\Gamma}{C_a}\right)\left(1 + \frac{D}{D_0}\right), \tag{A.4}$$

$$= \left\{1 - \frac{1}{m}\left(1 - \frac{\Gamma}{C_a}\right)\right\} - \left\{\frac{1}{mD_0}\left(1 - \frac{\Gamma}{C_a}\right)\right\}D. \tag{A.5}$$

Note that Eq. (A.5) is synonymous with Eq. (4).

References

[1] Allan RP, Ringer MA, Slingo A. Evaluation of moisture in the Hadley Centre climate model using simulations of HIRS water-vapour channel radiances. Quart J R Meteorol Soc 2003;129:3371–89.
[2] Aphalo PJ, Jarvis PG. Do stomata respond to relative humidity? Plant Cell Environ 1991;14:127–32.
[3] Bruijnzeel LA. Hydrology of moist tropical forests and effects of conversion: a state of knowledge review. UNESCO: International Hydrological Programme; 1990.
[4] Campbell GS, Norman JM. An introduction to environmental biophysics. 2nd ed.. New York: Springer-Verlag; 1998.
[5] Choudhury B, DiGirolamo NE, Susskind J, Darnell WL, Gupta SK, Asrar G. A biophysical process-based estimate of global land surface evaporation using satellite and ancillary data, II. Regional and global patterns of seasonal and annual variations. J Hydrol 1998;205:186–204.
[6] Collatz GJ, Ball JT, Grivet C, Berry JA. Regulation of stomatal conductance and transpiration: a physiological model of canopy processes. Agric For Meteorol 1991;54:107–36.
[7] Ellsworth DS. CO_2 enrichment in a maturing pine forest: are CO_2 exchange and water status in the canopy affected? Plant Cell Environ 1999;22:461–72.
[8] Ellsworth DS, Oren R, Huang C, Phillips N, Hendrey GR. Leaf and canopy responses to elevated CO_2 in a under free-air CO_2 enrichment. Oecologia 1995;104:139–46.
[9] Fan SM, Wofsy SC, Bakwin PS, Jacob DJ. Atmosphere–biosphere exchange of CO_2 and O_3 in the central Amazon forest. J Geophys Res 1990;95(D10):16851–64.
[10] Food and Agriculture Organization. Forest Resources Assessment 1990—Tropical Countries. Rome: FAO Forestry Paper 112; 1993.
[11] Gordon C, Cooper C, Senior CA, Banks H, Gregory JM, Johns TC, et al. The simulation of SST, sea ice extents and ocean heat transports in a version of the Hadley Centre coupled model without flux adjustments. Climate Dynam 2000;16:147–68.
[12] Grace J, Lloyd J, McIntyre J, Miranda A, Meir P, Miranda H, et al. Fluxes of carbon dioxide and water vapour over an undisturbed tropical forest in south-west Amazonia. Glob Change Biol 1995;1:1–12.
[13] Grace J, Malhi Y, Higuchi N, Meir P. Productivity of tropical forests. In: Roy J, Saugier B, Mooney HA, editors. Terrestrial global productivity. San Diego: Academic Press; 2001. p. 401–26.
[14] Grace J, Malhi Y, Lloyd J, McIntyre J, Miranda AC, Meir P, et al. The use of eddy covariance to infer the net carbon dioxide uptake of Brazilian rain forest. Glob Change Biol 1996;2:209–17.
[15] Griffin KL, Tissue DT, Turnbull MH, Whitehead D. The onset of photosynthetic acclimation to elevated CO_2 partial pressure in field-growth *Pinus radiata* D.Don after 4 years. Plant Cell Environ 2001;23:1089–98.
[16] Hikosaka K, Murakami A, Hirose T. Balancing carboxylation and regeneration of ribulose-1,5-bis-phosphate in leaf photosyn-

thesis: temperature acclimation of an evergreen tree, *Quercus myrsinaefolia*. Plant Cell Environ 1999;22:841–9.
[17] Hodnett MG, da Silva LP, da Rocha HR, Senna RC. Seasonal soil water storage changes beneath central Amazonian rainforest and pasture. J Hydrol 1995;170:233–54.
[18] Houghton JT, Callander BA, Varney SK, editors. Climate change 1992: The supplementary report to the IPCC scientific assessment. Cambridge: Cambridge University Press; 1992.
[19] Houghton JT, Ding Y, Griggs DJ, Noguer M, van der Linden PJ, Xiaosu D, editors. Climate change 2001: The scientific basis. Cambridge: Cambridge University Press; 2001.
[20] Houghton RA, Hackler JL. Emissions of carbon from forestry and land-use change in tropical Asia. Glob Change Biol 1999;5:481–92.
[21] Ingram WJ. On the robustness of the water vapor feedback: GCM vertical resolution and formulation. J Climate 2002;15:917–21.
[22] Inoue T, Nakamura K, Salamah S, Abbas I. Population dynamics of animals in unpredictably-changing tropical environments. J Biosci 1993;18:425–55.
[23] Ishizuka S, Tanaka S, Sakurai K, Hirai H, Hirotani H, Ogino K, et al. Characterization and distribution of soils at Lambir Hills National Park in Sarawak, Malaysia, with special reference to soil hardness and soil texture. Tropics 1998;8:31–44.
[24] Katul GG, Ellsworth DS, Lai C-T. Modelling assimilation and intercellular CO_2 from measured conductance: a synthesis of approaches. Plant Cell Environ 2000;23:1313–28.
[25] Kelliher FM, Luening R, Raupach MR, Schulze E-D. Maximum conductances for evaporation from global vegetation types. Agric For Meteorol 1995;73:1–16.
[26] Kumagai T, Katul GG, Saitoh TM, Sato Y, Manfroi OJ, Morooka T, et al. Water cycling in a Bornean tropical rain forest under current and projected precipitation scenarios. Water Resour Res 2004;40:W01104, doi:10.1029/2003WR002226.
[27] Kumagai T, Kuraji K, Noguchi H, Tanaka Y, Tanaka K, Suzuki M. Vertical profiles of environmental factors within tropical rainforest, Lambir Hills National Park, Sarawak, Malaysia. J For Res 2001;6:257–64.
[28] Kumagai T, Saitoh TM, Sato Y, Morooka T, Manfroi OJ, Kuraji K, et al. Transpiration, canopy conductance and the decoupling coefficient of a lowland mixed dipterocarp forest in Sarawak, Borneo: dry spell effects. J Hydrol 2004;287:237–51.
[29] Kumagai T, Saitoh TM, Sato Y, Takahashi H, Manfroi OJ, Morooka T, et al. Annual water balance and seasonality of evapotranspiration in a Bornean tropical rainforest. Agric For Meteorol, in press.
[30] Laio F, Porporato A, Ridolfi L, Rodriguez-Iturbe I. Plants in water-controlled ecosystems: active role in hydrologic processes and response to water stress. II. Probablistic soil moisture dynamics. Adv Water Res 2001;24:707–23.
[31] Lean J, Warrilow DA. Simulation of the regional climatic impact of Amazonian deforestation. Nature 1989;342:411–3.
[32] Leuning R. Modeling stomatal behaviour and photosynthesis of *Eucalyptus grandis*. Aust J Plant Physiol 1990;17:159–75.
[33] Leuning R. A critical appraisal of a combined stomatal-photosynthesis model for C_3 plants. Plant Cell Environ 1995;18:339–55.
[34] Lichter J, Lavine M, Mace KA, Richter DD, Schlesinger WH. Throughfall chemistry in a loblolly pine plantation under elevated atmospheric CO_2 concentrations. Biogeochem 2000;50:73–93.
[35] Lloyd J, Grace J, Miranda AC, Meir P, Wong SC, Miranda HS, et al. A simple calibrated model of Amazon rainforest productivity based on leaf biochemical properties. Plant Cell Environ 1995;18:1129–45.
[36] Lockwood JG. Is potential evapotranspiration and its relationship with actual evapotranspiration sensitive to elevated atmospheric CO_2 levels?. Climate Change 1999;41:193–212.
[37] Malhi Y, Baldocchi DD, Jarvis PG. The carbon balance of tropical, temperate and Boreal forests. Plant Cell Environ 1999;22:715–40.
[38] Malhi Y, Grace J. Tropical forests and atmospheric carbon dioxide. Trends Ecol Evol 2000;15:332–7.
[39] Malhi Y, Nobre AD, Grace J, Kruijt B, Pereira MGP, Culf A, et al. Carbon dioxide transfer over a Central Amazonian rain forest. J Geophys Res 1998;107(D20):31593–612.
[40] Malhi Y, Pegoraro E, Nobre AD, Pereira MGP, Grace J, Culf AD, et al. Energy and water dynamics of a central Amazonian rain forest. J Geophys Res 2002;107:8061, doi:10.1029/2001JD000623.
[41] Manfroi OJ, Kuraji K, Tanaka N, Suzuki M, Nakagawa M, Nakashizuka T, et al. The stemflow of trees in a Bornean lowland tropical forest. Hydrol Process 2004;18:2455–74.
[42] Meir P, Grace J. Scaling relationships for woody tissue respiration in two tropical rain forests. Plant Cell Environ 2002;25:963–73.
[43] Monteith JL. A reinterpretation of stomatal responses to humidity. Plant Cell Environ 1995;18:357–64.
[44] Niklaus PA, Splinger D, Korner C. Soil moisture dynamics of calcareous grassland under elevated CO_2. Oecologia 1998;117:201–8.
[45] Nobre CA, Sellers PJ, Shukla J. Amazonian deforestation and regional climate change. J Climate 1991;4:957–88.
[46] Norman JM. Simulation of microclimate. In: Hatfield JL, Thompson I, editors. Biometeorology and integrated pest management. New York: Academic Press; 1982. p. 65–99.
[47] Oren R, Ellsworth DS, Johnsen KH, Phillips N, Ewers BE, Maier C, et al. Soil fertility limits carbon sequestration by forest ecosystems in a CO_2-enriched atmosphere. Nature 2001;411:469–72.
[48] Oren R, Sperry JS, Ewers BE, Pataki DE, Phillips N, Megonigal JP. Sensitivity of mean canopy stomatal conductance to vapor pressure deficit in a flooded *Taxodium distichum* L. forest: hydraulic and non-hydraulic effects. Oecologia 2001;126:21–9.
[49] Oren R, Sperry JS, Katul GG, Pataki DE, Ewers BE, Phillips N, et al. Survey and synthesis of intra- and interspecific variation in stomatal sensitivity to vapour pressure deficit. Plant Cell Environ 1999;22:1515–26.
[50] Paegle J. Interactions between convective and large-scale motions over Amazonia. In: Dickinson RE, editor. The geophysiology of Amazonia. New York: John Wiley; 1987. p. 347–87.
[51] Pataki DE, Oren R, Tissue D. Elevated carbon dioxide does not affect canopy stomatal conductance of *Pinus taeda* L. Oecologia 1998;117:47–52.
[52] Porporato A, D'Odorico P, Laio F, Ridolfi L, Rodriguez-Iturbe I. Ecohydrology of water-controlled ecosystems. Adv Water Res 2002;25:1335–48.
[53] Priestley CHB, Taylor RJ. On the assessment of surface heat flux and evaporation using large-scale parameters. Mon Weather Rev 1972;100:81–92.
[54] Rodriguez-Iturbe I, Porporato A, Ridolfi L, Isham V, Cox DR. Probabilistic modelling of water balance at a point: the role of climate, soil and vegetation. Proc R Soc Lond A 1999;455:3789–805.
[55] Rogers A, Ellsworth DS. Photosynthetic acclimation of *Pinus taeda* (loblolly pine) to long-term growth in elevated pCO_2 (FACE). Plant Cell Environ 2002;25:851–8.
[56] Sakurai K. Soils and agriculture in Borneo. Tropics (in Japanese with English abstract) 1999;9:27–40.
[57] Saxe H, Cannell MGR, Johnsen O, Ryan MG, Vourlitis G. Tree and forest functioning in response to global warming. New Phytologist 2001;149:369–400.
[58] Schäfer KVR, Oren R, Ellsworth DS, Lai C-T, Herrick JD, Finzi AC, et al. Exposure to an enriched CO_2 atmosphere alters carbon assimilation and allocation in a pine forest ecosystem. Glob Change Biol 2003;9:1378–400.

[59] Schäfer KVR, Oren R, Lai C-T, Katul GG. Hydrologic balance in an intact temperate forest ecosystem under ambient and elevated atmospheric CO_2 concentration. Global Change Biol 2002;8: 895–911.

[60] Schulze E-D, Kelliher FM, Körner C, Lloyd J, Leuning R. Relationships among maximum stomatal conductance, ecosystem surface conductance, carbon assimilation rate, and plant nitrogen nutrition: a global ecology scaling exercise. Annu Rev Ecol Syst 1994;25:629–60.

[61] Seneviratne SI, Pal JS, Eltahir EAB, Schar C. Summer dryness in a warmer climate: a process study with a regional climate model. Climate Dynamics 2002;20:69–85.

[62] Shuttleworth WJ, Gash JHC, Lloyd CR, Moore CJ, Roberts JM, Marques Filho AdO, et al. Eddy correlation measurements of energy partition for Amazonian forest. Quart J R Meteorol Soc 1984;110:1143–62.

[63] Skole D, Tucker C. Tropical deforestation and habitat fragmentation in the Amazon: satellite data from 1978 to 1988. Science 1993;260:1905–10.

[64] Vourlitis GL, Priante Filho N, Hayashi HMS, Nogueira JdS, Caseiro FT, Campelo JJH. Seasonal variations in the net ecosystem CO_2 exchange of a mature Amazonian transitional tropical forest (cerradão). Funct Ecol 2001;15:388–95.

[65] Vourlitis GL, Priante Filho N, Hayashi HMS, Nogueira JdS, Caseiro FT, Campelo JJH. Seasonal variations in the evapotranspiration of transitional tropical forest of Mato Grosso, Brazil. Water Resour Res 2002;38(6), doi:10.1029/2000WR000122.

[66] Wong SC, Cowan IR, Farquhar GD. Stomatal conductance correlates with photosynthetic capacity. Nature 1979;282:424–6.

[67] Wullschleger SD, Norby RJ. Sap velocity and canopy transpiration in a sweetgum stand exposed to free-air CO_2 enrichment (FACE). New Phytologist 2001;150:489–98.

[68] Yamakura T, Kanzaki M, Itoh A, Ohkubo T, Ogino K, Chai EOK, et al. Forest architecture of Lambir rain forest revealed by a large-scale research plot. In: Lee H-S, Ashton PS, Ogino K, editors. Reports of new program for promotion of basic sciences. Studies of global environmental changes with special reference to Asia and Pacific regions, vol. II-3. Long term ecological research of tropical rain forest in Sarawak. Matsuyama: Ehime University, Japan; 1995. p. 2–20.

[69] Ye B, Del Genio AD, Lo KKW. CAPE variations in the current climate and in a climate change. J Climate 1998;11:1997–2015.